Materials Characterization 136 (2018) 407–416

Contents lists available at ScienceDirect

Materials Characterization

journal homepage: www.elsevier.com/locate/matchar

Structural transition from two-dimensional ZIF-L to three-dimensional ZIF-8 nanoparticles in aqueous room temperature synthesis with improved CO_2 adsorption

Imran Ullah Khan[a,b,c], Mohd Hafiz Dzarfan Othman[a,*], A.F. Ismail[a], N. Ismail[a], Juhana Jaafar[a], Haslenda Hashim[a], Mukhlis A. Rahman[a], Asim Jilani[a,d]

[a] Advanced Membrane Technology Research Centre (AMTEC), Faculty of Chemical and Energy Engineering, Universiti Teknologi Malaysia, 81310 Skudai, Johor, Malaysia
[b] School of Chemical and Material Engineering (SCME), National University of Science and Technology (NUST), H-12 Islamabad, Pakistan
[c] Process System Engineering Centre (PROSPECT), Faculty of Chemical and Energy Engineering, Universiti Teknologi Malaysia, 81310 Skudai, Johor, Malaysia
[d] Center of Nanotechnology, King Abdul-Aziz University, 21589 Jeddah, Saudi Arabia

ARTICLE INFO

Keywords:
Rapid synthesis
Particle size
Molar ratio
Transition
Basicity
Desorption

ABSTRACT

A new micron-sized leaf- two-dimensional (2D) structured zeolitic imidazolate framework (ZIF-L) and nano-sized ZIF-8 were successfully synthesised in aqueous basic solution at room temperature with the same molar ratio of reagents (Zn^{+2}/Hmim = 8). Both ZIFs have attracted tremendous research interest due to their wide applications including absorption, separation, and catalysis. This phase and morphology change could be tailored by changing the concentration of base-type additive triethylamine (TEA). Also, this morphology change from 2D (ZIF-L) to three-dimensional (3D) (ZIF-8) was observed by X-ray diffraction (XRD), transmission electron microscopy (TEM), field emission scanning electron microscopy (FESEM), thermogravimetric analysis (TGA), attenuated total reflectance infrared (ATR-IR) spectroscopy analysis, and surface area and pore textural properties using micromeritics gas adsorption analyser. The total amount of basic sites and carbon dioxide (CO_2) desorption capacity were also calculated using CO_2 temperature-programmed desorption (CO_2-TPD) technique. Furthermore, TEA/total mole ratio of 0.0006 was proved as transition loading between two phases. Also, the particle and crystal size of samples decreased with increasing TEA/total mole ratio. The smallest ZIF-L and ZIF-8 particles obtained were 1.6 μm and 177 nm, respectively that showed excellent thermal stability. The basicity and uptakes of CO_2 improved proportionally with TEA and followed this order: ZIF-8 > ZIF-L. This study provides some new insights into zeolitic imidazolate framework by controlling crystal growth and morphology.

1. Introduction

Zeolitic imidazolate frameworks (ZIFs) are a new subclass of metal-organic frameworks (MOFs) and emerge as a new family of molecular sieves and porous structure. The highly diversified structures, tunable pore sizes, and versatile functionalities inspired many researchers to explore its different industrial applications such as CO_2 adsorption [1], catalysis [2], membrane fabrication for gas separation [3], and gas storage [4,5]. Common metal sites used for synthesis of ZIFs are Zn^{+2} and Co^{+2} and there are many types of imidazole-type linkers like imidazole (IM), 1-methylimidazole (mIM), 2-methylimidazole (Hmim), 1-ethylimidazole (eIM), and 2-nitroimidazole (nIM). The combination of different metal sites and imidazole ligands would result in different structures and properties of ZIFs [6]. Solvothermal method and microwave-assisted are the most versatile approaches and to the best of our knowledge, most types of MOFs can be synthesised through these methods [6,7,8]. Despite the maturity of the process, both approaches suffer from high energy requirement while utilising expensive organic solvent in highly diluted manner [9,10]. Contradictory, aqueous system synthesis is reported to provide economical, rapid, nano-sized, and higher yield of formation compared to solvothermal and microwave-assisted synthesis [9,11]. Up to date, only limited types of MOFs have been successfully synthesised in aqueous solution because most organic ligands are insoluble in water [12,13].

Among the MOFs, ZIF-L and ZIF-8 have been documented to be well compatible with aqueous system synthesis. Nonetheless, MOFs are well-developed porous compounds but ZIFs are still in their infancy, such as crystal growth and pore structure. Recently, many researchers have synthesised and characterised various types of ZIFs particles [2–4,13–32]. Liquid-phase diffusion in methanol process is used for the

* Corresponding author.
E-mail address: hafiz@petroleum.utm.my (M.H.D. Othman).

https://doi.org/10.1016/j.matchar.2018.01.003
Received 20 October 2017; Received in revised form 30 December 2017; Accepted 1 January 2018
Available online 05 January 2018
1044-5803/

production of ZIFs crystals [28,29] but it takes many days to produce it. Zhang et al. [33] identified that Co/Hmim molar ratio played an important and crucial role in the synthesis of ZIF-L-Co with leaf-like structure. They also concluded that lower concentration of reactants gave larger particle size and vice versa. Pan et al. [34] replaced the organic solvent with water during the synthesis of ZIF-8 at room temperature and the resultant ZIF-8 nanoparticles showed excellent thermal stability. However, the requirement of the high molar ratio of zinc salt and organic ligand (1:70) makes this process costly and hazardous. Despite the different approaches that have been used for tuning the crystal shape and morphology of ZIFs, far less effort has been employed to the economical, friendly, and fast synthesis of ZIFs for CO_2 adsorption.

ZIF-L and ZIF-8 have many similarities that provides a unique opportunity to investigate their crystal growth during the synthesis such as both have the same reagents, i.e., zinc salt and Hmim [22,31]. Also, similar CO_2 adsorption capacity makes them promising materials for purification of natural gas [4]. A 2D ZIF-L is made up of the same building blocks as ZIF-8 [28] and have been widely used in various separation processes as an adsorbent to remove hazardous wastes such as dyes, aromatics, arsenic, and heavy metals [35], gas detachment, heterogeneous catalysis, drug delivery, and sensors [36].

The objective of this work is to investigate the effect of base type additive (TEA) on the morphology of ZIFs and CO_2 adsorption performance. Besides, critical loading of TEA that was used for intermediate structure between ZIF-L and ZIF-8 was identified during the synthesis process. Also, its influence on their CO_2 adsorption capacity would be reported and discussed here. The temperature programmed desorption (TPD) is the best technique to calculate basicity and CO_2 adsorption/desorption behaviour of porous materials [37]. To the best of our knowledge, the presented CO_2-TPD results for ZIF-L and ZIF-8 are the first experimental evidence of basicity calculations.

2. Experimental Section

2.1. Materials

The materials used to synthesise ZIF-L were zinc nitrate hexahydrate ($Zn(NO_3)_2{\cdot}6H_2O$, 99% purity), an organic linker, 2-methylimidazole (Hmim, 99% purity), and base-type additive triethylamine (TEA, 99.5% purity) to change its structure. All chemicals were purchased from Sigma-Aldrich and used without any further purification.

2.2. Synthesis of ZIF-L and ZIF-8

The synthesis of ZIF-L was described in literature [1,28] while some changes were done in this work to enhance the yield, decrease the chemical usage and improved desorption capacity. Briefly, the key synthesis parameters were the ratio of Hmim/zinc ion molar ratio (e.g., 8) and TEA/total mole ratio of the reactants. Approximately 2.95 g (1.98 mmol) of $Zn(NO_3)_2{\cdot}6H_2O$ and 6.5 g (15.83 mmol) of Hmim were dissolved in 200 mL of deionised water. Various amounts of TEA were added to Hmim solution as the deprotonation agent as shown in Table 1. Then, the aqueous solution of $Zn(NO_3)_2{\cdot}6H_2O$ was added into the aqueous solution of Hmim with stirring. The mixture was stirred at room temperature at various time intervals. The product was obtained by repeated centrifugation (10,000 rpm for 10 min), washed by deionised water to remove residual chemicals, and then dried in an oven at 60 °C for 12 h. The products ZIF-L (A0, A1, A2, and A3) were obtained at TEA/total mole ratios of 0, 0.0002, 0.0003, and 0.0005, respectively. Also, A4 and A5 represented transition stage. Meanwhile, ZIF-8 samples (A6 and A7) were also obtained when the TEA/total mole ratios of the reactants were increased up to 0.001 and 0.002, respectively. The yield of the products was measured using Eq. (1) and reported in Table 1.

Table 1
Different TEA/total mole ratio, yield and time for the synthesis of ZIL-L and ZIF-8.

Sample	TEA/total mole ratio	TEA volume (mL)	Duration of synthesis (min)	Yield (%)	Product
A0	0	0	240 [23]	90	ZIF-L
A1	0.0002	0.5	60	80	ZIF-L
A2	0.0003	1	60	90	ZIF-L
A3	0.0005	1.5	60	90	ZIF-L
A4	0.0006	2	60	80	Transition phase
A5	0.0009	3	60	80	Transition phase
A6	0.001	4	60	80	ZIF-8
A7	0.002	5	60	90	ZIF-8

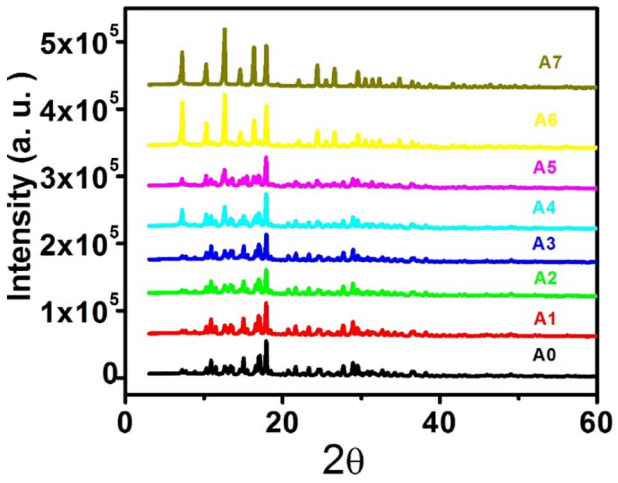

Fig. 1. XRD pattern of the synthesised samples with different TEA/total mole ratios: A0 (0), A1 (0.0002), A2 (0.0003), A3 (0.0005), A4 (0.0006), A5 (0.0009), A6 (0.001), and A7 (0.002).

$$\text{Yield (\%)} = \frac{\text{ZIF} - \text{L or ZIF} - 8\ \text{(obtained)}}{\text{ZIF} - \text{L or ZIF} - 8\text{(theoretical)}} \times 100 \quad (1)$$

2.3. Characterization

2.3.1. Physicochemical Analysis

The field emission scanning electron microscopy (FESEM) images were taken using a Hitachi SU 8020 microscope. The X-ray diffraction (XRD) analysis was performed on a Rigaku smart lab diffractometer using CuKα radiation at 40 KV and 30 mA in the 2θ range of 3°–100°. The attenuated total reflectance infrared (ATR−IR) spectroscopy analysis was performed using IRTracer-100 (Single Reflection Diamond for Spectrum Two, Shimadzu) to observe the functional groups of the synthesised ZIF-8 samples. The thermogravimetric analysis (TGA, Q 500, TA Instrument, USA) was used to check the thermal stability of the synthesised samples at different TEA loadings. TGA recorded the weight changes of the sample when heated from 30 to 900 °C at a heating rate of 10 °C/min under nitrogen atmosphere. The flow rate of N_2 was used up to 40 mL/min. The specific BET surface area, pores textural properties of the synthesised samples, and nitrogen adsorption-desorption isotherms were measured using Micromeritics gas adsorption analyser ASAP 2010 instrument equipped with a commercial software for calculation and analysis.

2.3.2. CO_2 Temperature Programmed Desorption (CO_2-TPD)

CO_2 temperature-programmed desorption tests were conducted to determine the total amount of basic sites on the surface of the ZIF-L and ZIF-8 samples. Experiments were carried out on Auto Chem II 2920

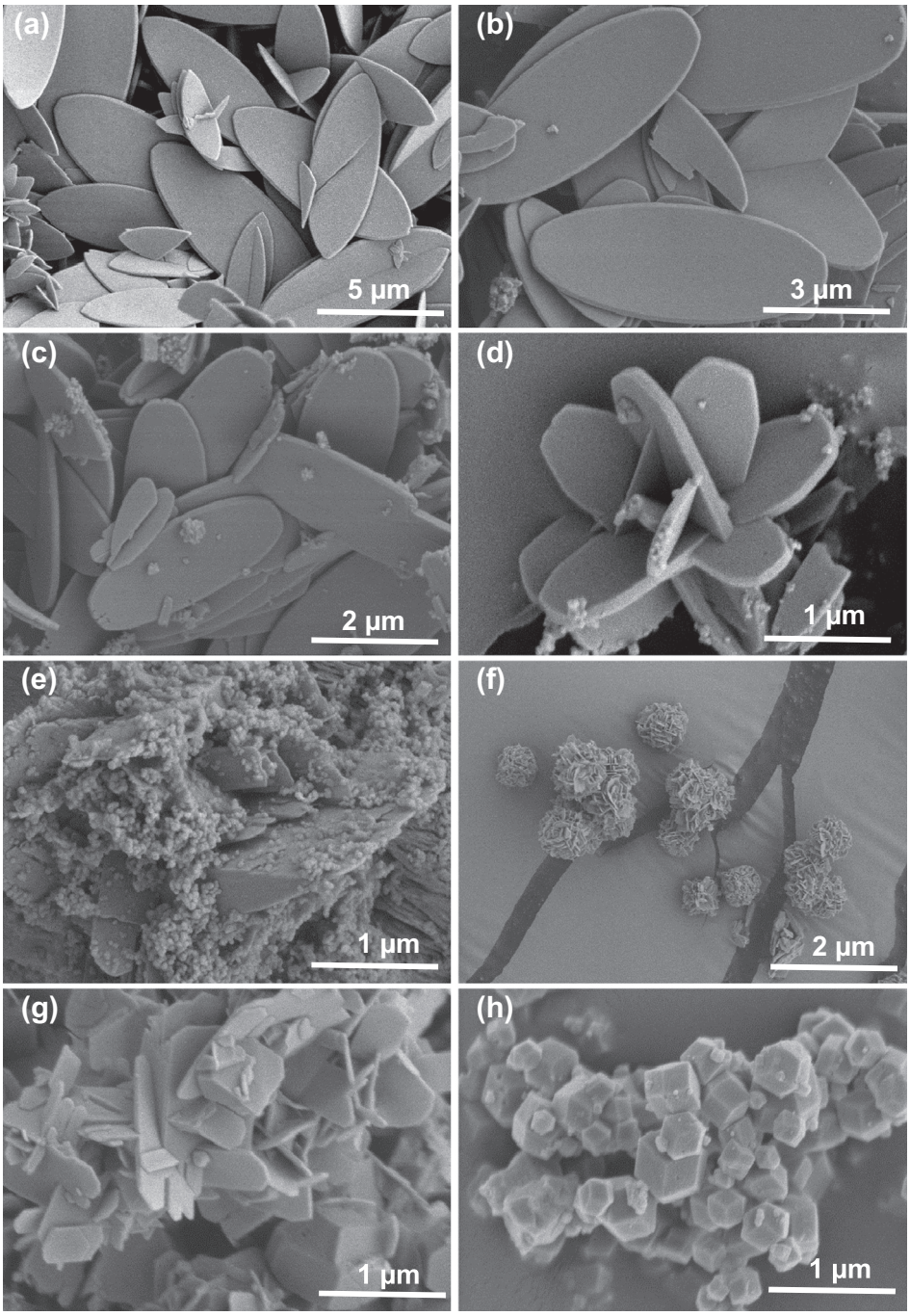

Fig. 2. FESEM images of the synthesised samples at different TEA/total mole ratios: (a) A0 (0), (b) A1 (0.0002), (c) A2 (0.0003), (d) A3 (0.0005), (e) A4 (0.0006), (f) A5 (0.0009), (g) A6 (0.001), and (h) A7 (0.002).

instrument equipped with a thermal conductivity detector (TCD) (Micromeritics, USA). Firstly, the sample was pretreated using Helium (He) with a flow rate of 30 mL/min at 150 °C for 2 h and then cooled to room temperature (50 °C). After that, the sample was saturated with CO_2 at a flow rate of 30 mL/min at 50 °C for 2 h. Following this adsorption, the sample was flushed with He at room temperature for 1.5 h to remove any physisorbed CO_2. After the He flush, the sample was heated at a heating rate of 10 °C/min with a He flow rate of 30 mL/min, and the desorbed CO_2 was measured by the Auto Chem II 2920 instrument with a TCD ramp to 900 °C. Effluent curves of CO_2 were recorded as CO_2-TPD curves. Finally, the surface basicity of the sample can be found out separately according to the amounts of desorbed CO_2. The amount of basic sites (mmol/g) was defined as the number of desorbed CO_2 molecules between room temperature and 900 °C during the TPD analysis. The amount of basic sites can be calculated from the area of the TPD spectrum as follows:

$$\text{Basicity} = \frac{A_{\text{sample}}}{A_{1\text{ mL}}\, m_{\text{sample}}} \times \frac{1}{V_m} \quad (2)$$

where basicity is the amount of basic sites (mmol/g), A_{sample} is the integrated area of the TPD spectrum of the sample, $A_{1\text{ mL}}$ is the area from the calibration pulse of 1 mL of CO_2, m_{sample} is the mass of the sample in grams, and V_m (mL/mmol) is the molar volume of CO_2 (0.0235 mL/mmol).

3. Results and Discussion

3.1. Structural and Surface Analysis

The X-ray diffraction (XRD) pattern for ZIF-L showed that the

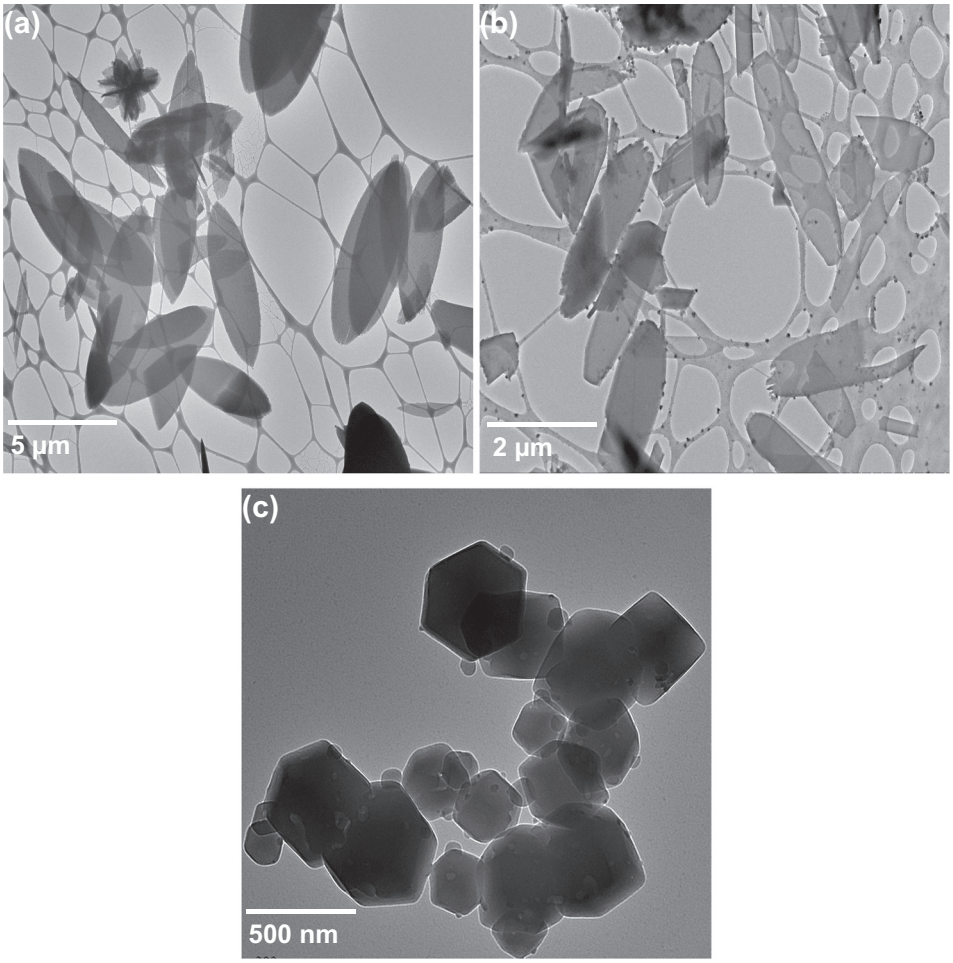

Fig. 3. TEM images of the synthesised samples with different TEA/total mole ratios: (a) A0 (0), (b) A3 (0.0005), and (c) A7 (0.002).

Table 2
Structural properties of the synthesised samples.

Sample	δ ± 0.0002	ε ± 0.0002	Crystal size (nm)	Particle size		Dimensions	
			Scherrer ± 1 nm	FESEM ± 2 nm	TEM ± 2 nm	Thickness(nm) ± 1 nm	Width (μm) ± 5 nm
A0	0.0015	0.0011	38	5.05 μm	5 μm	137	2.1
A1	0.0017	0.0011	38	3.2 μm	–	89	1.2
A2	0.0018	0.0011	36	3 μm	–	88	1.2
A3	0.0014	0.0010	35	1.6 μm	1.7 μm	77	0.77
A4	0.0021	0.0012	40	–	–	–	–
A5	0.0027	0.0013	41	–	–	–	–
A6	0.00071	0.00091	47	501 nm	–	–	–
A7	0.00087	0.00084	45	177 nm	181 nm	–	–

intensity of the peaks are in well agreement to the previous reported work [22,38,39]. In the first attempt (Fig. 1, A0), ZIF-L was synthesised in zinc salt and Hmim aqueous solution at room temperature with no addition of TEA. After continuous stirring, the synthesis solution turned cloudy that showed the occurrence of a reaction between the reactants. FESEM image (Fig. 2a) also confirmed the leaf-like structure of ZIF-L. However, a longer time of synthesis (4 h) was required due to low reaction rate and insufficient deprotonation of Hmim. When the small amounts of TEA (0.5, 1, and 1.5 mL which were equivalent to TEA/total mole ratios of0.0002, 0.0003, and 0.0005, respectively) were added in the synthesis solution, ZIF-L particles were formed after 60 min (Fig. 1, A1, A2 and A3). Furthermore, their FESEM images confirmed the leaf-like particles with 2D crystalline structure (Fig. 2b, c and d). The possible reason was the fast deprotonation of Hmim to produce more reactive sites for the reaction with Zn^{+2} [13,40,41]. Thus, ZIF-L was successfully synthesised in shorter time with high yield (Table 1). But, when the volume of TEA was increased up to 2 and 3 mL in the synthesis solution (TEA/total mole ratios of 0.0006 and 0.0009, respectively), the intensity of the characteristics peaks in the XRD analysis (Fig. 1, A4 and A5) increased, and FESEM images (Fig. 2e and f) clearly exhibited the transition stage of ZIF-L to ZIF-8 and the leaf-like structure started to break up. Higher TEA/total mole ratio increased the reaction rate by rapid deprotonation of Hmim, leading to the breakdown of the leaf-like structure. When the concentration of TEA in the synthesis solution was increased to 4 mL, the intensity of the peaks increased and showed almost similar curve as reported for ZIF-8 [12,23,35]. But FESEM image (Fig. 2g) was not fully confirmed the structure of ZIF-8. It suggested that 4 mL of TEA was still not sufficient to deprotonate Hmim for the formation of ZIF-8. When the volume of TEA was increased up to 5 mL, the characteristic peaks of ZIF-8 for the

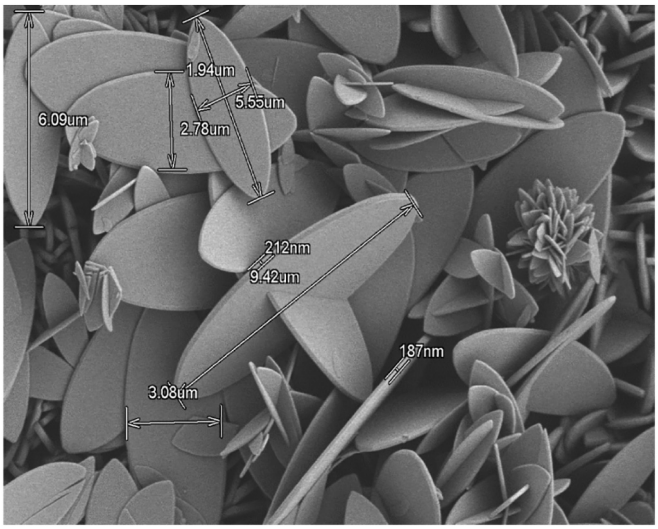

Fig. 4. Size, width, and thickness measurements of ZIF-L from FESEM images.

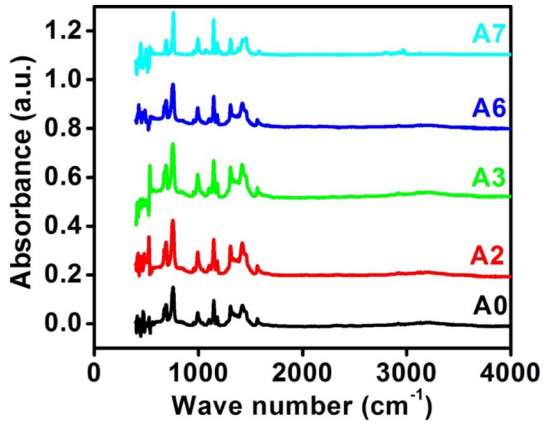

Fig. 5. ATR-IR spectrum analysis of the synthesised samples with different TEA/total mole ratios: A0 (0), A1, A2 (0.0003), A3 (0.0005), A6 (0.001), and A7 (0.002).

planes {110}, {200}, {211}, {222}, {310}, {222}, {321}, {411}, {420}, {332}, and {422} were clearly observed at 2θ of 7.24, 10.29, 12.64, 14.61, 16.37, 17.95, 19.38, 22.05, 23.01, 24.43, and 25.53, respectively. The intensity of the peaks are in good agreement with the XRD phase recognition DB card number for ZIF-8 (00-062-1030) and previously reported work [42,43]. Furthermore, FESEM image also confirmed the cubic hexagonal particle with 3D crystalline structure of pure ZIF-8 (Fig. 2h).

The structure of ZIF-L and ZIF-8 was further confirmed by the transmission electron microscopy (TEM) images (Fig. 3) that well agreed with the FESEM images. For this purpose, three samples (A0, A3, and A7) were selected for TEM analysis. These TEM images clearly exhibited the 2D leaf-like structure of ZIF-L without TEA, with the TEA/total mole ratio of 0.0005, and 3D hexagonal and octahedron morphology of ZIF-8 at high TEA loading (TEA/total mole ratio of 0.002).

The crystal size of the synthesised samples was calculated using Debye-Scherrer equation shown in Eq. (3) [44] and the series of FESEM and TEM images were used to estimate the average particle size of the synthesised samples (Table 2). Almost the same particle size was observed in FESEM and TEM images. It was identified that the particle size of ZIF-L samples decreased from 5.05 to 1.60 μm and the crystal size was also decreased from 38 to 35 nm (Table 2) when the TEA/total mole ratio was increased from 0 to 0.0005 as shown in Table 1. This reduction in particle size was due to the rapid deprotonation of Hmim at higher TEA loading, subsequently, producing more reactive sites on the organic ligands to ease the chemical reaction with the zinc salt. But when the TEA/total mole ratio was increased up to 0.0006 and 0.0009, the crystal size suddenly increased because of the transition stage as stated earlier. Also, it was not possible to measure the particle size in the transition stage because of breakage and irregularity as shown in Fig. 2e and f. After the transition stage, ZIF-8 nanoparticles were observed and their crystal and particle sizes decreased from 47 to 45 nm and 501 to 177 nm, respectively. This reduction in particle size was also due to the rapid deprotonation of Hmim at higher TEA loading.

$$D = \frac{0.9\lambda}{B \cdot \cos\theta} \tag{3}$$

where,

D = crystal size (nm),
B = full-width at half maximum of the peak in radian,
θ = measured diffraction angle of the peak, and.
λ = X-ray wavelength of CuKα (0.1542 nm).

Moreover, the dislocation density (δ) is measured using Eq. (4) [45] where D is the crystal size.

$$\delta = \frac{1}{D^2} \tag{4}$$

This gives more insight into the quantity of defects in the crystals. Very small defects are found in ZIF-L particles that slightly increased with the decreasing size of the particles from A0 to A7 as shown in Table 2. Strain-induced broadening arising from crystal imperfections and distortion calculated using Eq. (5) are related with lattice strains [46]. The lattice strain was smaller and almost constant for ZIF-L but slightly higher for ZIF-8 nanoparticles due to the rapid reaction at higher TEA loading (Table 2).

$$\varepsilon = \frac{\beta \cos\theta}{4} \tag{5}$$

Other structural parameters for ZIF-L particles like average thickness and width were also measured using the FESEM images of ZIF-L.

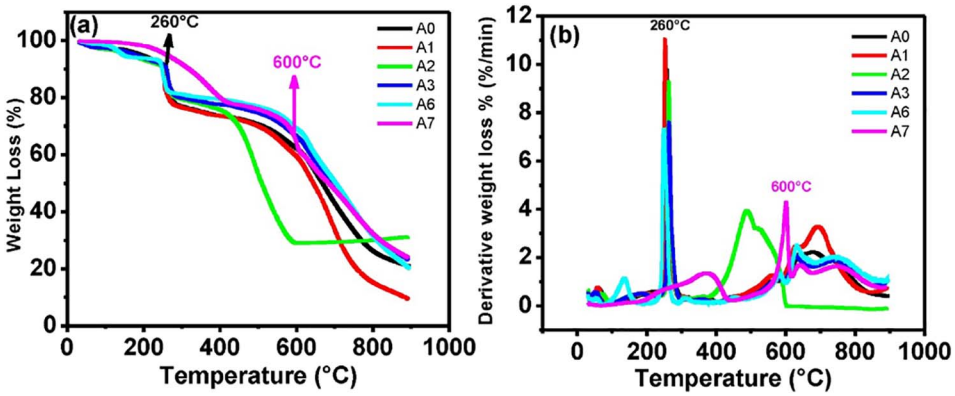

Fig. 6. (a) Thermal stability of the synthesised samples with weight loss profile at various temperatures with different TEA/total mole ratios: A0 (0), A1 (0.0002), A2 (0.0003), A3 (0.0005), A6 (0.001), and A7 (0.002) (b) Thermal stability of the synthesised samples with derivative of weight loss profile at various temperatures with different TEA/total mole ratios.

Table 3
The pore textural properties of the prepared samples.

Sample	BET surface area (m^2/g)	Langmuir surface area (m^2/g)	Micropore volume (cm^3/g)	Mesopore volume (cm^3/g)	Micropore area (m^2/g)
A0 (100 °C)	2.5	3.6	0.0001	0.0033	0.1
A0 (200 °C)	133	210	0.0026	0.011	7.7
A1 (100 °C)	–	–	–	–	–
A1 (200 °C)	135	213	0.0044	0.013	11.5
A2 (100 °C)	–	–	–	–	–
A2 (200 °C)	163	238	0.0085	0.16	22
A3 (100 °C)	2.6	3	0.0004	0.0016	0.88
A3 (200 °C)	166	251	0.0059	0.18	15
A4 (100 °C)	–	–	–	–	–
A4 (200 °C)	212	235	0.074	0.04	193
A6 (100 °C)	–	–	–	–	–
A6 (200 °C)	525	602	0.18	0.08	448
A7 (100 °C)	431	528	0.1341	0.083	339
A7 (200 °C)	1472	1605	0.5543	0.0524	1441

One image is shown in Fig. 4 to explain how thickness and width of the samples were measured. It is clear that both parameters are dependent on particle size, where it decreased with the decrease in particle size (Table 2).

3.2. Functional Groups

ATR–IR spectra observed bond stretching vibration of different functional groups at various frequencies. To check the effect of TEA on ZIF-L, three samples with minimum (A0), medium (A2) and maximum (A3) amount of TEA were considered, as shown in Fig. 5. These spectra showed the vibrations of imidazolate and zinc ion units because of their bond origin, basic and acidic nature It was observed that the spectra of all samples showed a good agreement with previous documented works [47,48]. The results for ZIF-L showed various peaks such as 423 cm^{-1} and 450 cm^{-1} due to Zn–N and Zn–O stretching, respectively, 1146–1307 cm^{-1} that is ascribed to C–H vibrations, 1384 cm^{-1} due to C–C stretching, 1500–1700 cm^{-1} that is associated to C=N stretching, and 1350–1500 cm^{-1} that is associated with the entire ring stretching [49]. The spectral bands in the region of 900–1350 cm^{-1} are for the alkane in-plane blending whereas the vibrations at 600–800 cm^{-1} are named as out of plane bending [40,50]. For ZIF-L and ZIF-8, the peak positions of the spectra are almost the same. The only difference is aromatic compounds (N-CH_3) vibration at 2800–2820 cm^{-1} and H bonded N–H at 3000 cm^{-1} due to the excess amount of TEA [51].

3.3. Thermal Stability

The thermal stability of the synthesised products of ZIF-L and ZIF-8 was measured by thermogravimetric analysis (TGA) in which the mass of the product was monitored as a function of temperature as shown in Fig. 6a. We reported the higher thermal stability of products compared to previous works [22,37,38,47]. All ZIF-L samples exhibited a quite gradual in weight losses initially and there were sudden weight losses at around 260 °C (Fig. 6a). As proven in FESEM (Fig. 2g) results that the TEA/total mole ratio of 0.001 was still not enough for the formation of ZIF-8, the TGA results for this sample also gave low stability, as sudden weight loss occurred at around 260 °C (Fig. 6a, sample A6). Meanwhile, pure ZIF-8 (A7) was highly stable as its sudden weight loss started at around 600 °C (Fig. 6a, sample A7).

Further verification of the thermal stability of these samples was done by calculating the derivative of the weight loss curves at different temperature (Fig. 6b). All the synthesised ZIF-L samples had two peaks representing two different weight loss temperatures or thermal events.

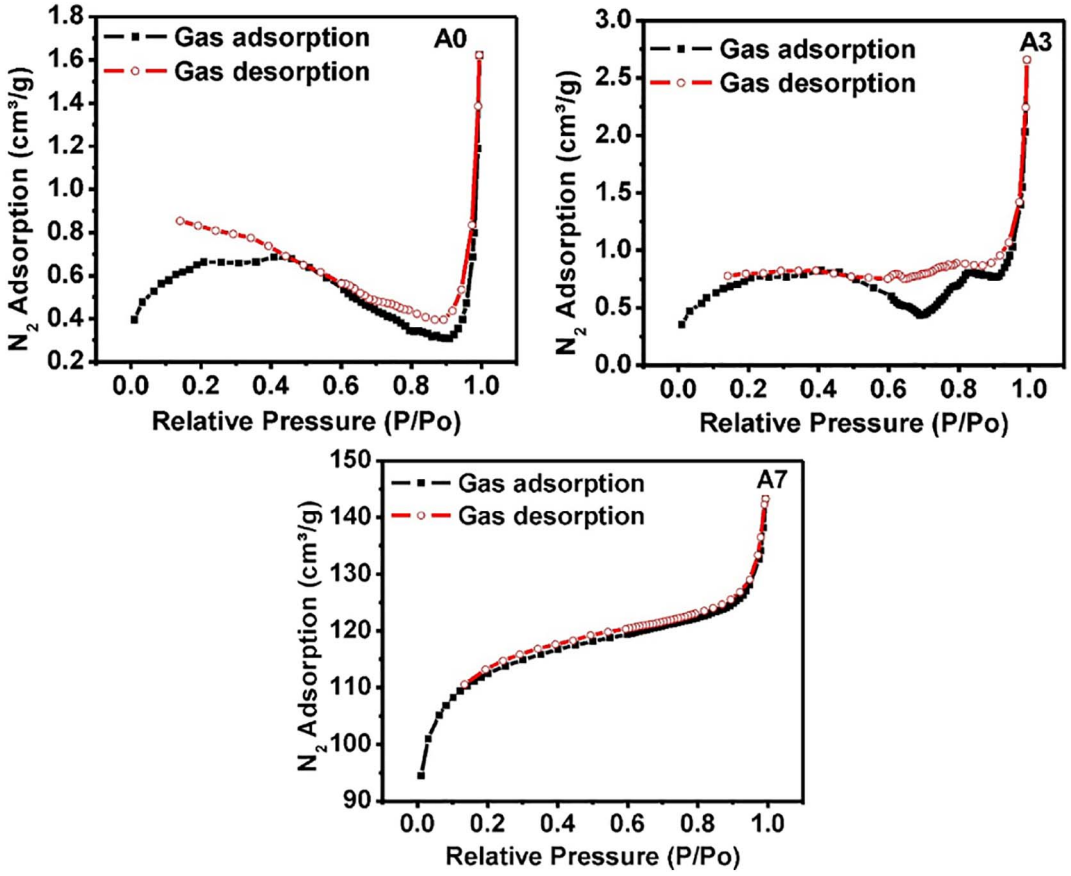

Fig. 7. Nitrogen sorption isotherms of the synthesised samples at 100 °C with different TEA/total mole ratios: A0 (0), A3 (0.0005), and A7 (0.002).

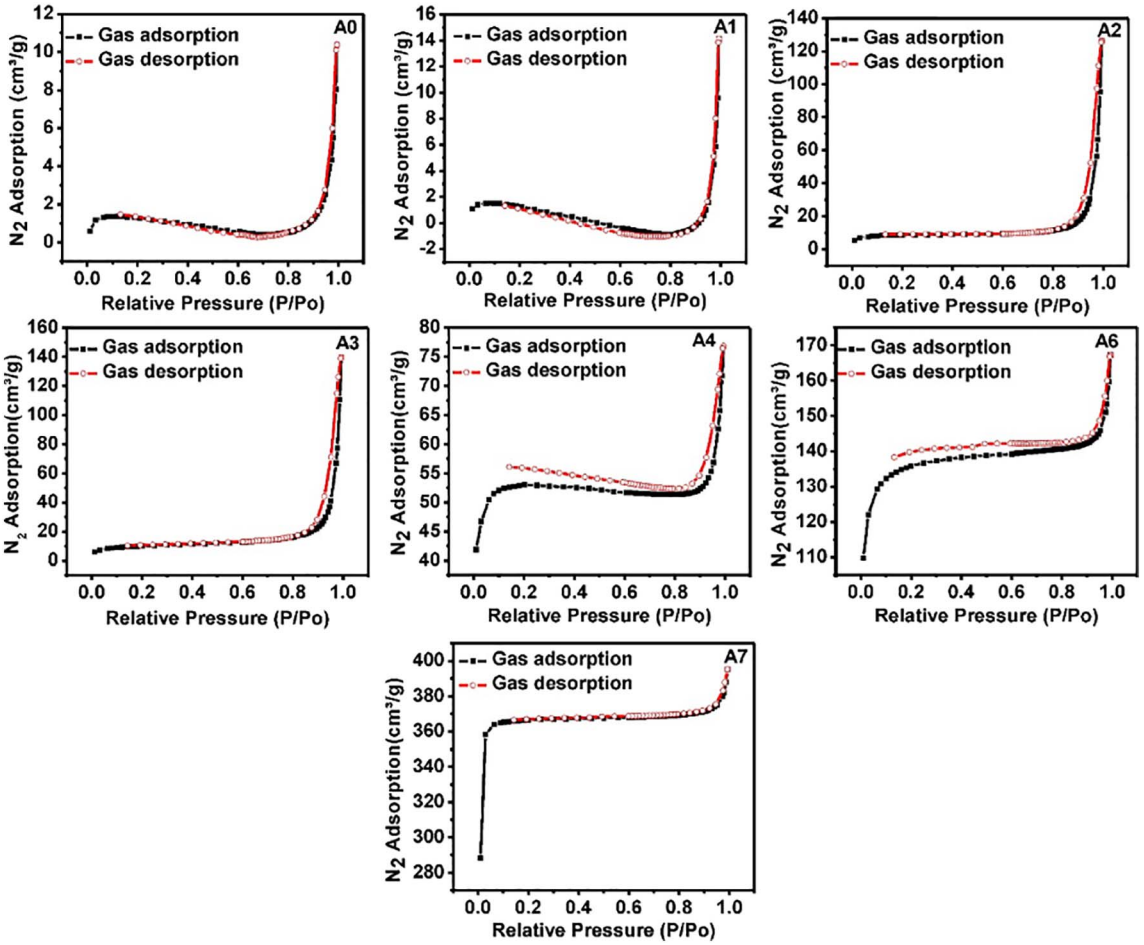

Fig. 8. Nitrogen sorption isotherms of the synthesised samples at 200 °C with different TEA/total mole ratios: A0 (0), A1 (0.0002), A2 (0.0003), A3 (0.0005), A4 (0.0006), A6 (0.001), and A7 (0.002).

The first derivative peak temperature (T_p) was around 100–150 °C which shows the initial weight loss and attributed to the evaporation of the trapped deionised water from the pores and unreactive species (e.g., Hmim) [5,21,31] and the carbonisation of organic ligand molecules in ZIF-L framework [47,50]. The second T_p (second weight loss) was in the range of 250 to 300 °C indicating the point of greatest rate of change on the weight loss curve and was due to the decomposition of organic linkers and ZIF-L crystal structure. However, ZIF-8 had three peaks representing three different weight loss temperatures or thermal events. The first derivative peak temperature (T_p) was around 100 °C which shows the initial weight loss and attributed to the evaporation of the trapped deionised water from the pores and unreactive species (e.g., Hmim). The second T_p (second weight loss) was in the range of 250 to 300 °C and it was associated to the carbonisation of organic ligand molecules in ZIF-8 framework. The third T_p (third weight loss) occurred at around 600 °C indicating the point of greatest rate of change on the weight loss curve and was due to the decomposition of organic linkers and ZIF-8 crystal structure.

3.4. Pore Textural Properties

The surface area is one of the major parameters for characterising porous materials. The pore textural properties of the synthesised samples are presented in Table 3. Samples A0 and A3 of ZIF-L and A7 of ZIF-8 were selected for BET analysis at 100 °C. Smaller BET and Langmuir surface areas of ZIF-L and ZIF-8 particles were found compared to previously reported works [23,34,52]. The reason for the low surface area was probably the incomplete activation of the samples at 100 °C. The pores of the samples still contained guest molecules and residual unreacted species which led to a decrease in the surface area [24]. Therefore, all samples of ZIF-L and ZIF-8 were heated at 200 °C in an oven to remove all the entrapped guest molecules. All surface properties were improved due to evaporation of guest molecules from the pores (Table 3). The results are in good agreement with the reported works [2,30,33].

Nitrogen sorption isotherms for as-synthesised samples (A0, A3, and A7) at 100 °C are shown in Fig. 7. It was observed that low gas adsorbed at 100 °C due to the low BET and Langmuir surface area, and micro- and mesoporosity of the samples (Table 3). Moreover, these samples have a rising trend of surface properties with decreasing size. Nitrogen sorption isotherms at 200 °C are shown in Fig.8. For all samples, it was observed that the gas absorbed even at a very low relative pressure, revealing the microporous structure of samples, while higher adsorption of gas at high relative pressure ($P/P_0 > 0.95$) indicates microporous and mesoporous structure. It was also identified that the amount of adsorbed gas in ZIF-L (A0–A3) samples increased from 10.5 to 141 cm^3/g due to the increase of all surface properties. As sample A4 was identified as transition stage between ZIF-L and ZIF-8, the low absorbance of gas also verifies this phenomenon (Fig.8, A4). Furthermore, the amount of the adsorbed gas in ZIF-8 (A6 and A7) samples increased from 168 to 397 cm^3/g due to the increase of surface areas and microporosity (Fig.8, A6 and A7). Moreover, typical Type I isotherms were obtained for all samples as shown in Fig. 8, which confirms their microporosity [53-56]. However, the behaviour of the isotherms for the values of $P/P_0 > 0.95$ changed to Type IV, which reveals the existence of large pores due to mesoporous structure [49].

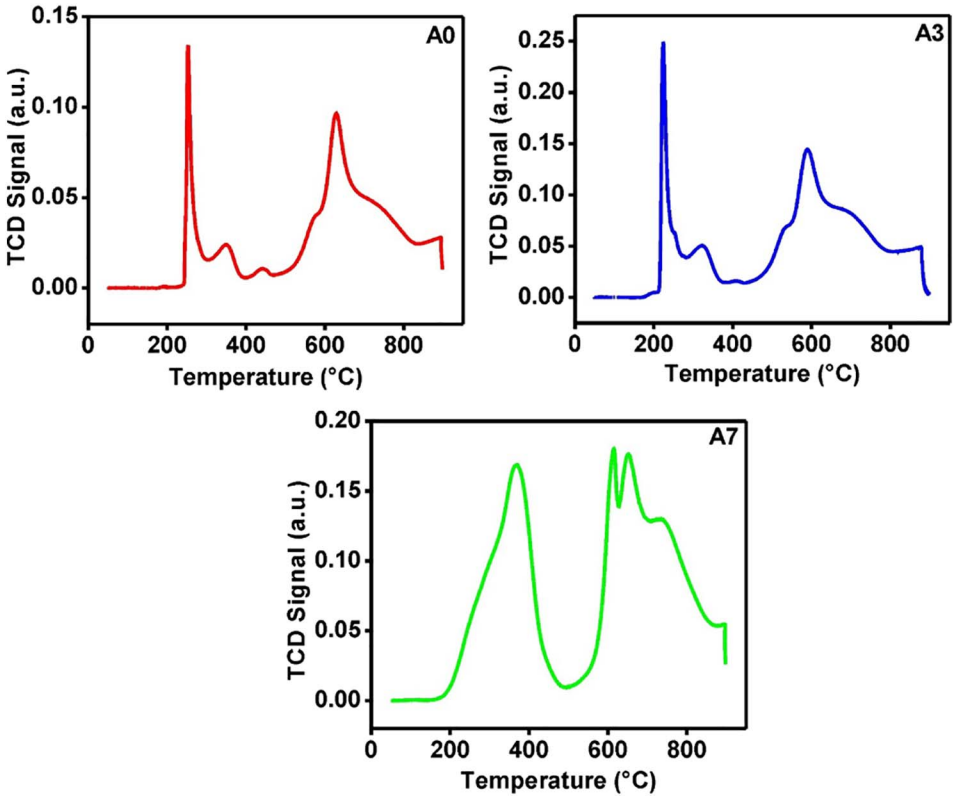

Fig. 9. CO_2-TPD spectra recorded for various samples between room temperature and 900 °C with different TEA/total mole ratios: A0 (0), A3 (0.0005), and A7 (0.002).

Table 4
Amounts of the basic surface sites of the ZIF-L and ZIF-8 crystals at various temperatures.

Sample	Temperature (°C)	Amount of basic sites (mmol/g)
A0	223.3	1.48
	264	4.54
	602.9	13.45
	868.3	1.30
Total		20.77
A3	252.8	1.82
	344.9	2.75
	439.4	1.45
	627.4	1.38
	647.7	13.80
Total		21.20
A7	115.4	0.018
	367.4	8.83
	614.4	2.52
	651	10.89
	894.3	0.477
Total		22.74

3.5. CO_2 Temperature Programmed Desorption (CO_2–TPD)

The total amount of desorbed CO_2 on the samples was calculated from the CO_2-TPD isotherms as shown in Fig. 9 using Eq. (2). Table 4 lists the amount of basic sites that increased after the appropriate addition of TEA. Two samples of ZIF-L with maximum (A0), and the minimum (A3) particle size were selected for TPD-CO_2 analysis as shown in Fig. 9. The calculated basic sites were quite high and impressive compared with the previously reported CO_2-TPD for ZIF-8 alkali-metal cation exchanged faujasite type zeolites [20,37]. The increased basicity is ascribed to the presence of amine basic groups in TEA which adsorbed more CO_2, an acidic molecule. Furthermore, ZIF-8 sample showed higher basicity compared to ZIF-L due to smaller particle size and high surface area and porosity as documented in Tables 2 and 3, respectively.

4. Conclusions

This study presents an alternative approach to produce ZIF-L with leaf-like structure and ZIF-8 cubic crystals in an aqueous solution at ambient temperature. The Zn^{+2}/Hmim ratio of 8 was used with various concentrations of TEA. It was concluded that TEA played an important role for the transition of morphology from ZIF-L to ZIF-8. It was identified that TEA/total mole ratio of 0.0005 and 0.002 played an important and most promising role in controlling the crystal growth, porosity, and CO_2 desorption of ZIF-L and ZIF-8. This phase transition process is very important and vital advancement in ZIFs formation is rarely reported. Furthermore, it controls the crystal growth and formation as it deprotonates the organic ligand. More importantly, TEA threshold loading of 2 mL which was responsible for the phase transition was determined. Furthermore, it was observed that BET surface area and porosity of samples were increased by heat treatment at 200 °C to remove the unreacted species in the pores and subsequently increased the adsorption capacity. Also, ZIF-L and ZIF-8 particles showed excellent thermal stability at around 260 and 600 °C, respectively. Additionally, ZIF-L and ZIF-8 particles showed a significant amount of basic sites on their surfaces due to the presence of TEA and thus improving the adsorption capacity and selectivity towards CO_2. Moreover, Zn^{+2}/Hmim ratio, TEA loading, and temperature are the major parameters to improve this synthesis process and adsorption of CO_2. Our research will undoubtedly provide a better understanding of crystal growth and morphology control of ZIFs during the synthesis process and help to improve the basicity and adsorption capacity for CO_2.

Acknowledgement

The authors gratefully acknowledge the financial support from Universiti Teknologi Malaysia under the Research University Grant Tier 1 (Project number: Q. J130000.2546.12H25) and Nippon Sheet Glass Foundation for Materials Science and Engineering under Overseas Research Grant Scheme (Project number: R. J130000.7346.4B218). The

authors would also like to thank Research Management Centre, Universiti Teknologi Malaysia for the technical support. Lastly, the first author would also like to thank National University of Science and Technology (NUST), Pakistan for their scholarship under Faculty Development Programme (FDP).

Refrences

[1] R. Chen, J. Yao, Q. Gu, S. Smeets, A two-dimensional zeolitic imidazolate framework with a cushion-shaped cavity for CO 2 adsorption, Chem. Commun. 48 (82) (2013) 9500–9502 http://pubs.rsc.org/en/content/articlehtml/2013/cc/c3cc44342f , Accessed date: 14 April 2016.

[2] G. Editors, J. Long, O. Yaghi, J. Lee, O.K. Farha, J. Roberts, K.A. Scheidt, S.T. Nguyen, J.T. Hupp, Metal–organic framework materials as catalysts, Chem. Soc. Rev. 38 (2009) 1450–1459, http://dx.doi.org/10.1039/b807080f.

[3] Z. Low, A. Razmjou, K. Wang, S. Gray, Effect of addition of two-dimensional ZIF-L nanoflakes on the properties of polyethersulfone ultrafiltration membrane, J. Memb. Sci. 460 (2014) 9–17 http://www.sciencedirect.com/science/article/pii/S0376738814001495 , Accessed date: 18 April 2016.

[4] W.-C. Lee, H.-T. Chien, Y. Lo, H.-C. Chiu, T. Wang, D.-Y. Kang, Synthesis of Zeolitic imidazolate framework core–shell nanosheets using zinc-imidazole pseudopolymorphs, ACS Appl. Mater. Interfaces 7 (2015) 18353–18361, http://dx.doi.org/10.1021/acsami.5b04217.

[5] B. Wang, A. Côté, H. Furukawa, M. O'Keeffe, O. Yaghi, Colossal cages in zeolitic imidazolate frameworks as selective carbon dioxide reservoirs, Nature. 453 (2008) 207–211 http://www.nature.com/nature/journal/v453/n7192/abs/nature06900.html , Accessed date: 22 May 2016.

[6] Y.R. Lee, J. Kim, W.S. Ahn, Synthesis of metal-organic frameworks: a mini review, Korean J. Chem. Eng. 30 (2013) 1667–1680, http://dx.doi.org/10.1007/s11814-013-0140-6.

[7] W. Kleist, M. Maciejewski, A. Baiker, MOF-5 based mixed-linker metal–organic frameworks: Synthesis, thermal stability and catalytic application, Thermochim. Acta. 499 (2010) 71–78, http://dx.doi.org/10.1016/j.tca.2009.11.004.

[8] C.-M. Lu, J. Liu, K. Xiao, A.T. Harris, Microwave enhanced synthesis of MOF-5 and its CO2 capture ability at moderate temperatures across multiple capture and release cycles, Chem. Eng. J. 156 (2010) 465–470, http://dx.doi.org/10.1016/j.cej.2009.10.067.

[9] Y. Yoo, H.-K. Jeong, Rapid fabrication of metal organic framework thin films using microwave-induced thermal deposition, Chem. Commun. (Camb) (2008) 2441–2443, http://dx.doi.org/10.1039/b800061a.

[10] J. Qian, F. Sun, L. Qin, Hydrothermal Synthesis of Zeolitic Imidazolate Framework-67 (ZIF-67) Nanocrystals, (2012), http://dx.doi.org/10.1016/j.matlet.2012.05.077.

[11] Y. Pan, D. Heryadi, F. Zhou, L. Zhao, G. Lestari, H. Su, Z. Lai, Tuning the crystal morphology and size of zeolitic imidazolate framework-8 in aqueous solution by surfactants, CrystEngComm 13 (2011) 6937, http://dx.doi.org/10.1039/c1ce05780d.

[12] A. Gross, E. Sherman, J. Vajo, Aqueous room temperature synthesis of cobalt and zinc sodalite zeolitic imidizolate frameworks, Dalt. Trans. 41 (18) (2012) 5458–5460 http://pubs.rsc.org/en/content/articlehtml/2012/dt/c2dt30174a , Accessed date: 22 May 2016.

[13] M. Jian, B. Liu, R. Liu, J. Qu, H. Wang, X. Zhang, Water-based synthesis of zeolitic imidazolate framework-8 with high morphology level at room temperature, RSC Adv. 5 (2015) 48433–48441, http://dx.doi.org/10.1039/C5RA04033G.

[14] X. Huang, Y. Lin, J. Zhang, X. Chen, Ligand-directed strategy for Zeolite-type metal–organic frameworks: zinc (II) imidazolates with unusual Zeolitic topologies, Angew. Chem. 118 (10) (2006) 1587–1589 http://onlinelibrary.wiley.com/doi/10.1002/ange.200503778/full , Accessed date: 21 May 2016.

[15] O.M. Banerjee R., A. Phan, B. Wang, C. Knobler, H. Furukawa, M. O'Keeffe, Yaghi, High-throughput synthesis of zeolitic imidazolate frameworks and application to CO2 capture, Science 319(5865) (80) (2008) 939–943 http://science.sciencemag.org/content/319/5865/939.short , Accessed date: 21 May 2016.

[16] R. Banerjee, H. Furukawa, D. Britt, C. Knobler, M. O'Keeffe, O.M. Yaghi, Control of pore size and functionality in isoreticular zeolitic imidazolate frameworks and their carbon dioxide selective capture properties, J. Am. Chem. Soc. 131 (2009) 3875–3877, http://dx.doi.org/10.1021/ja809459e.

[17] J. Cravillon, R. Nayuk, S. Springer, A. Feldhoff, K. Huber, M. Wiebcke, Controlling Zeolitic imidazolate framework nano- and microcrystal formation: insight into crystal growth by time-resolved in situ Static light scattering, Chem. Mater. 23 (2011) 2130–2141, http://dx.doi.org/10.1021/cm103571y.

[18] D. Fairen-Jimenez, Opening the gate: framework flexibility in ZIF-8 explored by experiments and simulations, J. Am. Chem. Soc. 133 (23) (2011) 8900–8902 http://pubs.acs.org/doi/abs/10.1021/ja202154j , Accessed date: 25 May 2016.

[19] Q. Shi, Z. Chen, Z. Song, Synthesis of ZIF-8 and ZIF-67 by steam-assisted conversion and an investigation of their tribological behaviors, Angew. Chem. Int. Ed. 50 (3) (2011), http://onlinelibrary.wiley.com/doi/10.1002/anie.201004937/full , Accessed date: 14 April 2016.

[20] Z. Zhang, S. Xian, H. Xi, H. Wang, Z. Li, Improvement of CO 2 adsorption on ZIF-8 crystals modified by enhancing basicity of surface, Chem. Eng. Sci. 66 (20) (2011) 4878–4888 http://www.sciencedirect.com/science/article/pii/S0009250911004374 , Accessed date: 23 May 2016.

[21] A. Bétard, R.A. Fischer, Metal-organic framework thin films: from fundamentals to applications, Chem. Rev. 112 (2012) 1055–1083, http://dx.doi.org/10.1021/cr200167v.

[22] Q. Song, S. Nataraj, M. Roussenova, Zeolitic imidazolate framework (ZIF-8) based polymer nanocomposite membranes for gas separation, Energy Environ. Sci. 5 (2012) 8359–8369 http://pubs.rsc.org/en/content/articlehtml/2012/ee/c2ee21996d , Accessed date: 20 May 2016.

[23] R. Chen, J. Yao, Q. Gu, S. Smeets, C. Baerlocher, H. Gu, D. Zhu, W. Morris, O.M. Yaghi, H. Wang, A two-dimensional zeolitic imidazolate framework with a cushion-shaped cavity for CO2 adsorption, Chem. Commun. (Camb) 49 (2013) 9500–9502, http://dx.doi.org/10.1039/c3cc44342f.

[24] K. Kida, M. Okita, K. Fujita, S. Tanaka, Y. Miyake, Formation of high crystalline ZIF-8 in an aqueous solution, CrystEngComm 15 (9) (2013) 1794–1801 http://pubs.rsc.org/en/content/articlehtml/2012/ce/c2ce26847g , Accessed date: 21 May 2016.

[25] D. Yamamoto, T. Maki, S. Watanabe, Synthesis and adsorption properties of ZIF-8 nanoparticles using a micromixer, Chem. Eng. J. 227 (2013) 145–150 http://www.sciencedirect.com/science/article/pii/S1385894712011308 , Accessed date: 25 May 2016.

[26] High-yield synthesis of zeolitic imidazolate frameworks from stoichiometric metal and ligand precursor aqueous solutions at room temperature, CrystEngComm 15 (18) (2013) 3601–3606 http://pubs.rsc.org/en/content/articlehtml/2013/ce/c3ce27093a (accessed May 21, 2016).

[27] B. Zornoza, C. Tellez, J. Coronas, J. Gascon, F. Kapteijn, Metal organic framework based mixed matrix membranes: an increasingly important field of research with a large application potential, Microporous Mesoporous Mater. 166 (2013) 67–78, http://dx.doi.org/10.1016/j.micromeso.2012.03.012.

[28] Z. Low, J. Yao, Q. Liu, M. He, Crystal transformation in zeolitic-imidazolate framework, Cryst. Growth Des. 14 (12) (2014) 6589–6598 http://pubs.acs.org/doi/abs/10.1021/cg501502r , Accessed date: 23 May 2016.

[29] Y. Wu, M. Zhou, B. Zhang, B. Wu, J. Li, J. Qiao, X. Guan, F. Li, Amino acid assisted templating synthesis of hierarchical zeolitic imidazolate framework-8 for efficient arsenate removal, Nanoscale 6 (2014) 1105–1112, http://dx.doi.org/10.1039/C3NR04390H.

[30] J. Yao, H. Wang, Zeolitic imidazolate framework composite membranes and thin films: synthesis and applications, Chem. Soc. Rev. 43 (2014) 4470–4493, http://dx.doi.org/10.1039/c3cs60480b.

[31] Z. Zhong, J. Yao, Z. Low, R. Chen, M. He, H. Wang, Carbon composite membrane derived from a two-dimensional zeolitic imidazolate framework and its gas separation properties, Carbon N. Y. 72 (2014) 242–249 http://www.sciencedirect.com/science/article/pii/S0008622314001304 , Accessed date: 14 April 2016.

[32] N. Nordin, S. Racha, T. Matsuura, Facile modification of ZIF-8 mixed matrix membrane for CO 2/CH 4 separation: synthesis and preparation, RSC Adv. 5 (54) (2015) 43110–43120 http://pubs.rsc.org/en/content/articlehtml/2015/ra/c5ra02230d , Accessed date: 18 May 2016.

[33] J. Zhang, T. Zhang, D. Yu, K. Xiao, Y. Hong, Transition from ZIF-L-Co to ZIF-67: a new insight into the structural evolution of zeolitic imidazolate frameworks (ZIFs) in aqueous systems, CrystEngComm 8 (2015) 5–8, http://dx.doi.org/10.1039/C5CE01531F.

[34] Y. Pan, Y. Liu, G. Zeng, L. Zhao, Z. Lai, Rapid synthesis of zeolitic imidazolate framework-8 (ZIF-8) nanocrystals in an aqueous system, Chem. Commun. 47 (7) (2011) 2071–2073 http://pubs.rsc.org/en/content/articlehtml/2011/cc/c0cc05002d , Accessed date: 22 May 2016.

[35] A. Mohd Nasir, N.A.H. Md Nordin, P.S. Goh, A.F. Ismail, Application of two-dimensional leaf-shaped Zeolitic imidazolate framework (2D ZIF-L) as arsenite adsorbent: kinetic, isotherm and mechanism, J. Mol. Liq. (2017), http://dx.doi.org/10.1016/j.molliq.2017.12.005.

[36] K. Gangu, S. Maddila, S.B. Mukkamala, S.B. Jonnalagadda, A review on contemporary metal-organic framework materials, Inorganica Chim. Acta. 446 (2016) 61–74, http://dx.doi.org/10.1016/j.ica.2016.02.062.

[37] O. Klepel, B. Hunger, Temperature-programmed desorption (TPD) of carbon dioxide on alkali-metal cation-exchanged faujasite type zeolites, J. Therm. Anal. Calorim. 80 (2005) 201–206, http://dx.doi.org/10.1007/s10973-005-0636-3.

[38] S. Haydar, C. Moreno-Castilla, M.A. Ferro-García, F. Carrasco-Marín, J. Rivera-Utrilla, A. Perrard, J.P. Joly, Regularities in the temperature-programmed desorption spectra of CO2 and CO from activated carbons, Carbon N. Y. 38 (2000) 1297–1308, http://dx.doi.org/10.1016/S0008-6223(99)00256-0.

[39] J. Yao, M. He, H. Wang, Strategies for controlling crystal structure and reducing usage of organic ligand and solvents in the synthesis of zeolitic imidazolate frameworks, CrystEngComm 17 (27) (2015) 4970–4976 http://pubs.rsc.org/en/content/articlehtml/2015/ce/c5ce00663e , Accessed date: 14 April 2016.

[40] M. He, J. Yao, Q. Liu, K. Wang, F. Chen, H. Wang, Facile synthesis of zeolitic imidazolate framework-8 from a concentrated aqueous solution, Microporous Mesoporous Mater. 184 (2014) 55–60, http://dx.doi.org/10.1016/j.micromeso.2013.10.003.

[41] Y. Hu, H. Kazemian, S. Rohani, Y. Huang, Y. Song, In situ high pressure study of ZIF-8 by FTIR spectroscopy, Chem. Commun. (Camb.) 47 (2011) 12694–12696, http://dx.doi.org/10.1039/c1cc15525c.

[42] C.W. Tsai, E.H.G. Langner, The effect of synthesis temperature on the particle size of nano-ZIF-8, Microporous Mesoporous Mater. 221 (2016) 8–13, http://dx.doi.org/10.1016/j.micromeso.2015.08.041.

[43] C.-W. Tsai, E.H.G. Langner, The effect of synthesis temperature on the particle size of nano-ZIF-8, Microporous Mesoporous Mater. 221 (2016) 8–13, http://dx.doi.org/10.1016/j.micromeso.2015.08.041.

[44] M.S. Abdel-wahab, A. Jilani, I.S. Yahia, A.A. Al-Ghamdi, Enhanced the photocatalytic activity of Ni-doped ZnO thin films: morphological, optical and XPS analysis, Superlattices Microstruct. 94 (2016) 108–118, http://dx.doi.org/10.1016/j.spmi.2016.03.043.

[45] A. Jilani, M.S. Abdel-wahab, A.A. Al-ghamdi, A. Sadik Dahlan, I.S. Yahia, Nonlinear optical parameters of nanocrystalline AZO thin film measured at different substrate

temperatures, Phys. B Condens. Matter 481 (2016) 97–103, http://dx.doi.org/10.1016/j.physb.2015.10.038.
[46] J. Tan, B. Civalleri, A. Erba, E. Albanese, Quantum mechanical predictions to elucidate the anisotropic elastic properties of zeolitic imidazolate frameworks: ZIF-4 vs. ZIF-zni, CrystEngComm 17 (2) (2015) 375–382 http://pubs.rsc.org/-/content/articlehtml/2015/ce/c4ce01564a , Accessed date: 9 September 2017.
[47] S. Xue, H. Jiang, Z. Zhong, Z.X. Low, R. Chen, W. Xing, Palladium nanoparticles supported on a two-dimensional layered zeolitic imidazolate framework-L as an efficient size-selective catalyst, Microporous Mesoporous Mater. 221 (2016) 220–227, http://dx.doi.org/10.1016/j.micromeso.2015.09.053.
[48] Q. Liu, Z.X. Low, Y. Feng, S. Leong, Z. Zhong, J. Yao, K. Hapgood, H. Wang, Direct conversion of two-dimensional ZIF-L film to porous ZnO nano-sheet film and its performance as photoanode in dye-sensitized solar cell, Microporous Mesoporous Mater. 194 (2014) 1–7, http://dx.doi.org/10.1016/j.micromeso.2014.03.023.
[49] Z. Zhang, S. Xian, H. Xi, H. Wang, Z. Li, Improvement of CO2 adsorption on ZIF-8 crystals modified by enhancing basicity of surface, Chem. Eng. Sci. 66 (2011) 4878–4888, http://dx.doi.org/10.1016/j.ces.2011.06.051.
[50] M. Shah, H.T. Kwon, V. Tran, S. Sachdeva, H.K. Jeong, One step in situ synthesis of supported zeolitic imidazolate framework ZIF-8 membranes: Role of sodium formate, Microporous Mesoporous Mater. 165 (2013) 63–69, http://dx.doi.org/10.1016/j.micromeso.2012.07.046.
[51] S. Tanaka, K. Kida, M. Okita, Y. Ito, Y. Miyake, Size-controlled synthesis of zeolitic imidazolate framework-8 (ZIF-8) crystals in an aqueous system at room temperature, Chem. Lett. 41 (2012) 1337–1339, http://dx.doi.org/10.1246/cl.2012.1337.
[52] N.A.H.M. Nordin, A.F. Ismail, A. Mustafa, P.S. Goh, D. Rana, T. Matsuura, Aqueous room temperature synthesis of zeolitic imidazole framework 8 (ZIF-8) with various concentrations of triethylamine, RSC Adv. 4 (2014) 33292, http://dx.doi.org/10.1039/C4RA03593C.
[53] J. Cravillon, S. Münzer, Rapid room-temperature synthesis and characterization of nanocrystals of a prototypical zeolitic imidazolate framework, Chem. Mater. 21 (8) (2009) 1410–1412 http://pubs.acs.org/doi/abs/10.1021/cm900166h , Accessed date: 25 May 2016.
[54] J. Qian, F. Sun, L. Qin, Hydrothermal synthesis of zeolitic imidazolate framework-67 (ZIF-67) nanocrystals, Mater. Lett. 82 (2012) 220–223 http://www.sciencedirect.com/science/article/pii/S0167577X12007550 , Accessed date: 25 May 2016.
[55] K.S. Park, Z. Ni, A.P. Cote, J.Y. Choi, R. Huang, F.J. Uribe-Romo, H.K. Chae, M. O'Keeffe, O.M. Yaghi, Exceptional chemical and thermal stability of zeolitic imidazolate frameworks, Proc. Natl. Acad. Sci. 103 (2006) 10186–10191, http://dx.doi.org/10.1073/pnas.0602439103.
[56] J. Rowsell, O. Yaghi, Metal–organic frameworks: a new class of porous materials, Microporous Mesoporous Mater. 73 (1) (2004) 3–14 http://www.sciencedirect.com/science/article/pii/S1387181104001295 , Accessed date: 13 September 2017.